Article

Developmental Cell

Transport properties of canonical PIN-FORMED proteins from *Arabidopsis* and the role of the loop domain in auxin transport

Graphical abstract

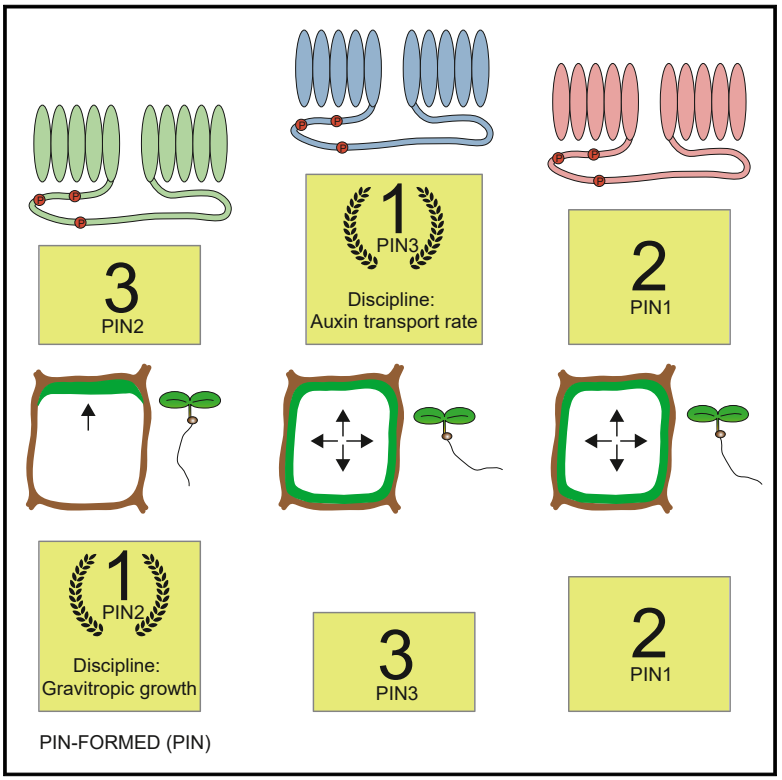

Authors

Dorina P. Janacek, Martina Kolb, Lukas Schulz, ..., Kirsten ten Tusscher, Claus Schwechheimer, Ulrich Z. Hammes

Correspondence

ulrich.hammes@tum.de

In brief

Polar auxin transport regulates plant growth responses, and Janacek et al. establish that PIN-FORMED auxin exporters have transport properties unique to every individual PIN. These properties depend on the interplay of transmembrane and loop domains to precisely fine-tune auxin flow to mediate growth responses.

Highlights

- PIN-FORMED auxin exporters have different transport properties
- The intrinsically disordered loop contributes to the transport process
- Properties of the loop domains are interchangeable between PINs
- Slow auxin transport in the *PIN2* domain is required for gravitropic root growth

Janacek et al., 2024, Developmental Cell *59*, 3259–3271
December 16, 2024
https://doi.org/10.1016/j.devcel.2024.09.020

CellPress

Developmental Cell

CellPress
OPEN ACCESS

Article

Transport properties of canonical PIN-FORMED proteins from *Arabidopsis* and the role of the loop domain in auxin transport

Dorina P. Janacek,[1] Martina Kolb,[1] Lukas Schulz,[1] Julia Mergner,[2,3] Bernhard Kuster,[2,3] Matouš Glanc,[4] Jiří Friml,[4] Kirsten ten Tusscher,[5] Claus Schwechheimer,[1] and Ulrich Z. Hammes[1,6,*]

[1]Plant Systems Biology, School of Life Sciences Weihenstephan, Technical University of Munich, 85354 Freising, Germany
[2]Proteomics and Bioanalytics, School of Life Sciences Weihenstephan, Technical University of Munich, 85954 Freising, Germany
[3]Bavarian Center for Biomolecular Mass Spectrometry (BayBioMS), School of Life Sciences Weihenstephan, Technical University of Munich, Freising, Germany
[4]Institute of Science and Technology Austria (IST Austria), 3400 Klosterneuburg, Austria
[5]Computational Developmental Biology, Department of Biology, Utrecht University, Utrecht, the Netherlands
[6]Lead contact
*Correspondence: ulrich.hammes@tum.de
https://doi.org/10.1016/j.devcel.2024.09.020

SUMMARY

The phytohormone auxin is polarly transported in plants by PIN-FORMED (PIN) transporters and controls virtually all growth and developmental processes. Canonical PINs possess a long, largely disordered cytosolic loop. Auxin transport by canonical PINs is activated by loop phosphorylation by certain kinases. The structure of the PIN transmembrane domains was recently determined, their transport properties remained poorly characterized, and the role of the loop in the transport process was unclear. Here, we determined the quantitative kinetic parameters of auxin transport mediated by *Arabidopsis* PINs to mathematically model auxin distribution in roots and to test these predictions *in vivo*. Using chimeras between transmembrane and loop domains of different PINs, we demonstrate a strong correlation between transport parameters and physiological output, indicating that the loop domain is not only required to activate PIN-mediated auxin transport, but it has an additional role in the transport process by a currently unknown mechanism.

INTRODUCTION

The phytohormone auxin (indole-3-acetic acid [IAA]) controls essentially all aspects of plant growth and development. Many developmental effects controlled by auxin require its redistribution within the plant by polar auxin transport.[1–8] Different types of transporters participate in the transport of IAA into and out of the cell.[9] Among these, PIN-FORMED (PIN) auxin exporters are the key players in polar auxin transport because several family members are polarly localized in the plasma membranes of many cells, thus providing directionality to IAA export.[9–11] Mutations in *PINs* cause well-defined phenotypes. Among others, the *pin1* mutant displays the eponymous pin-shaped inflorescence,[12] the *pin2* mutant has agravitropic root growth,[13] and the *pin3 pin4 pin7 (pin347)* triple mutant is non-phototropic.[14]

Recently, the structures of PIN1, PIN3, and PIN8 were elucidated by cryoelectron microscopy (cryo-EM).[15–17] PINs were shown to transport IAA by a crossover elevator uniport mechanism using the membrane potential as a driving force.[18] PINs form dimers, with each monomer consisting of 10 transmembrane helices (M) separated by a hydrophilic loop domain between M5 and M6. The PIN monomer can be divided into a scaffold domain, comprising the first two helices of each bundle (M1-M2 and M6-M7) and a transport domain comprising the remaining helices in two three-helix bundles with the characteristic crossover between the broken helices M4 and M9 at the center (M3-M4a/b-M5 and M8-M9a/b-M10).[18]

The cytoplasmic loop between M5 and M6 in PINs can be used to non-phylogenetically classify the PINs into long-loop (or canonical) PINs and short-loop (or non-canonical) PINs. In *Arabidopsis* PINs, the long loop ranges between 297 aa in PIN4 and 329 aa in PIN2 while the short loop is 29 aa in PIN5 and 44 aa in PIN8. *Arabidopsis thaliana* PIN6 possesses a loop of intermediate size (250 aa). Unfortunately, none of the recent structures was able to determine the loop structure except for a short ~40 aa β sheet domain directly following M5 in PIN1 and PIN3.[15,17] The intermediate PIN6 and short loop PIN8 are able to transport IAA constitutively.[16,19] In contrast, transport activity of canonical PINs is under the control of automatic gain control (AGC)1 and AGC3 kinases, suggesting that parts of the long loop are by default autoinhibitory, and phosphorylation is required to overcome this inhibition.[16,20,21] Several AGCVIII

kinase mutants display auxin-related phenotypes. Particularly, higher-order mutants of *D6 PROTEIN KINASE (D6PK)* and its three closest relatives *(D6PK-LIKE1-D6PKL-3; D6PKs)* as well as mutants of *PINOID (PID)* display undifferentiated inflorescences, similar to *pin1* mutants, suggesting a role in polar auxin transport.[22–24] At least five serine residues (S1–S5) within the loop are critical targets for PIN phosphorylation and activation by D6PK and PID.[21] S1–S3 are embedded in highly conserved repeated TPRXS sequence motifs, whereas the sequence contexts of the S4 and S5 residues are more variable.[25] Despite the recent progress made by determining the PIN structures, the transport properties of canonical PINs, particularly the impact of the loop on substrate transport and its phosphorylation status, remained elusive. In this study, we show that canonical PINs display distinct transport properties. We show that transport properties additionally depend on the identity of the activating kinase. We further show that the transport properties of the individual PINs, combined with their localization and polarity, critically impact the physiological role of PINs. Finally, our data demonstrate that the loop is not only critical for transport activation but also through its interaction with the transmembrane domains, it contributes to the transport process itself and determines transport rates.

RESULTS

Transport properties of canonical PINs

Knowledge about the biochemical parameters of auxin transport by individual PINs is crucial to improve existing models of auxin transport for precise predictions about plant growth and future studies. Several studies have modeled IAA fluxes but in the absence of biochemical parameters assumed identical transport properties for all PINs.[5,26] Recent data obtained for PIN1, PIN3, and PIN8 found unexpectedly high and divergent dissociation constant (K_D) values (IAA binding constants) of ~200, 100, and 40 μM, respectively, indicating that PINs possess different affinities for their substrates.[15–17] Furthermore, it was not known if the activating kinases impact PIN transport properties. We previously established a *Xenopus laevis* oocyte-based export system that allows controlling the initial substrate concentration in the cells precisely by injecting defined substrate concentrations.[21,27] Using this system, we initially determined the IAA transport rates in the linear range for the canonical PINs, both without kinase and combined with D6PK or PID in *Xenopus laevis* oocytes at an internal concentration of 1 μM (Figures 1A–1I). We found that all canonical PINs were inactive without kinase and were activated significantly ($p < 0.03$) by PID. In contrast to PIN2, PIN1 and PIN3 were also activated by D6PK ($p < 0.02$) at this concentration, but the transport rates were only significantly different ($p < 0.05$) between activation by D6PK and PID for PIN2 and PIN3 (Figures 1D–1F). Since we found that the transport properties of the phylogenetically closely related and genetically redundant PIN3, PIN4, and PIN7 were more similar to each other than to those of the other canonical PINs, we limited the subsequent analyses to PIN3 as a representative member (Figures 1G–1I).[7,14,28]

We determined the IAA transport rates mediated by PIN1, PIN2, and PIN3 as a function of the internal IAA concentration using the range between 0.2 and 10 μM[29] (Figures 2A, 2D, and 2G). We found that over this concentration range, all PINs tested were unable to transport IAA in the absence of a kinase, and all PINs could be activated by D6PK as well as by PID. For all PIN/kinase combinations investigated, we found a linear correlation between IAA concentration and transport rates. This indicates that PINs possess a very low substrate affinity (high K_m) and that the kinetics at physiological IAA concentrations are below K_m in the seemingly linear range of the Michaelis-Menten curve. Transport rates of PIN3 were 4 times higher than transport rates of PIN1, which were about twice as high as those of PIN2. This shows that canonical PINs possess different transport rates. Since we know from recent work that a Michaelis-Menten model can describe substrate binding, we compared the fit of our data with a linear model versus a Michaelis-Menten model (Table S1).[15–17] We found that in the case of PIN3 in combination with D6PK, the Michaelis-Menten model was indeed preferred and revealed a K_m of 143.3 μM, albeit with rather low confidence. Nevertheless, this value is in good agreement with the K_D of PIN3 for IAA (160.4 μM) observed by surface plasmon resonance (SPR).[15] For PIN1 and PIN2 with both kinases and PIN3 with PINOID, the linear model was preferred. This indicates that the substrate affinity of PIN3 co-expressed with PID is even lower than that of PIN3 with D6PK. This may also be the case for PIN1 and PIN2, but it is also possible that the comparison was not possible due to the lower transport rates and, consequently, the lower signal-to-noise ratio of these transporters, compared with PIN3. Together, these results support the notion that PINs indeed have substrate affinities that are much lower than the physiological concentration of IAA and operate in the linear transport range.

To rule out that these differences were due to differences in protein levels, we determined the amount of transporter, kinase, and phosphorylation level in oocytes at the onset of the experiment by liquid chromatography-tandem mass spectrometry (LC-MS/MS) (Figure S1). We found that the abundance of transporters and kinases were very similar and therefore ruled out differences in protein levels as the reason for their different transport rates (Figures S1A, S1C, and S1E). We next investigated if the differences are due to PIN phosphorylation and examined PIN phosphorylation at all serine and threonine residues of the PIN1, PIN2, and PIN3 intracellular loops by phosphoproteomic measurements (Figures S1B, S1D, and S1F). Some of the serine residues corresponded to the previously studied S1–S5, whereas others fit the RXS consensus for putative D6PK and PID target sites.[9] The general phosphorylation pattern in oocytes and in plants, as observed in the *Arabidopsis* phosphoproteome, showed significant overlap but also differences and should not be compared directly.[30] The kinase-dependent phosphorylation patterns differed between PIN1, PIN2, and PIN3, but phosphorylation at the critical S1–S5 residues was in line with these sites being phosphorylated by D6PK and PID.[21,31,32] Generally, phosphorylation by D6PK and PID was qualitatively and quantitatively very similar on all PINs, suggesting that differences in the transport rates between kinases are likely not due to differential phosphorylation (Figures S1B, S1D, and S1F). We found that PIN2 contained the highest number of phosphorylated residues but displayed the lowest transport rates. This indicates that transport rates and the number of phosphorylated residues are not correlated, at least not in our system.

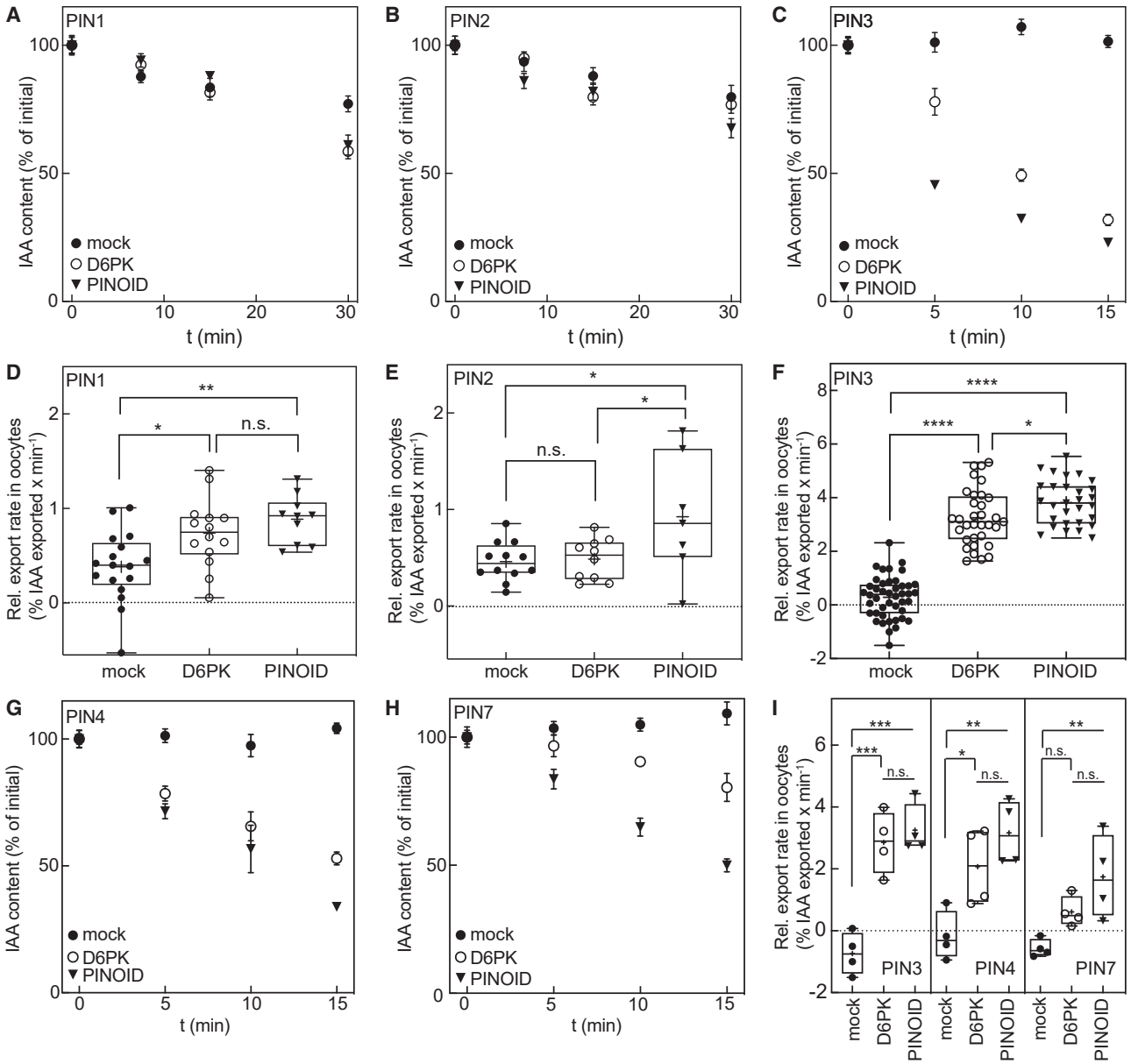

Figure 1. IAA transport properties of canonical PINs in *Xenopus* oocytes

(A) Representative time course experiments for PIN1 expressed without (●), with D6PK (○), or with PID (▼). Time points are mean and SE.

(B) Representative time course experiments for PIN2 expressed without (●), with D6PK (○), or with PID (▼). Time points are mean and SE.

(C) Representative time course experiments for PIN3 expressed without (●), with D6PK (○), or with PID (▼).

(D) Relative IAA export rates for PIN1 at $[IAA_{in}]$ = 1 μM.

(E) Relative IAA export rates for PIN2 at $[IAA_{in}]$ = 1 μM.

(F) Relative IAA export rates for PIN3 at $[IAA_{in}]$ = 1 μM. Boxplots range from the 25th to 75th percentile, and the median is shown; the mean is represented by (+). Groups were compared by one-way ANOVA, followed by Tukey's post hoc test.

(G) Representative time course experiments for PIN4 expressed without (●), with D6PK (○), or with PID (▼). Time points are mean and SE.

(H) Representative time course experiments for PIN7 expressed without (●), with D6PK (○), or with PID (▼). Time points are mean and SE.

(I) Relative IAA export rates at [1 μM] $[IAA_{in}]$ = 1 μM for PIN3, PIN4, and PIN7. Boxplots range from the minimum to maximum percentile, and the median is shown; the mean is represented by (+). Groups were compared by one-way ANOVA, followed by Tukey's post hoc test. Data points are mean and SE. Details on statistics and sample sizes are shown in Table S2.

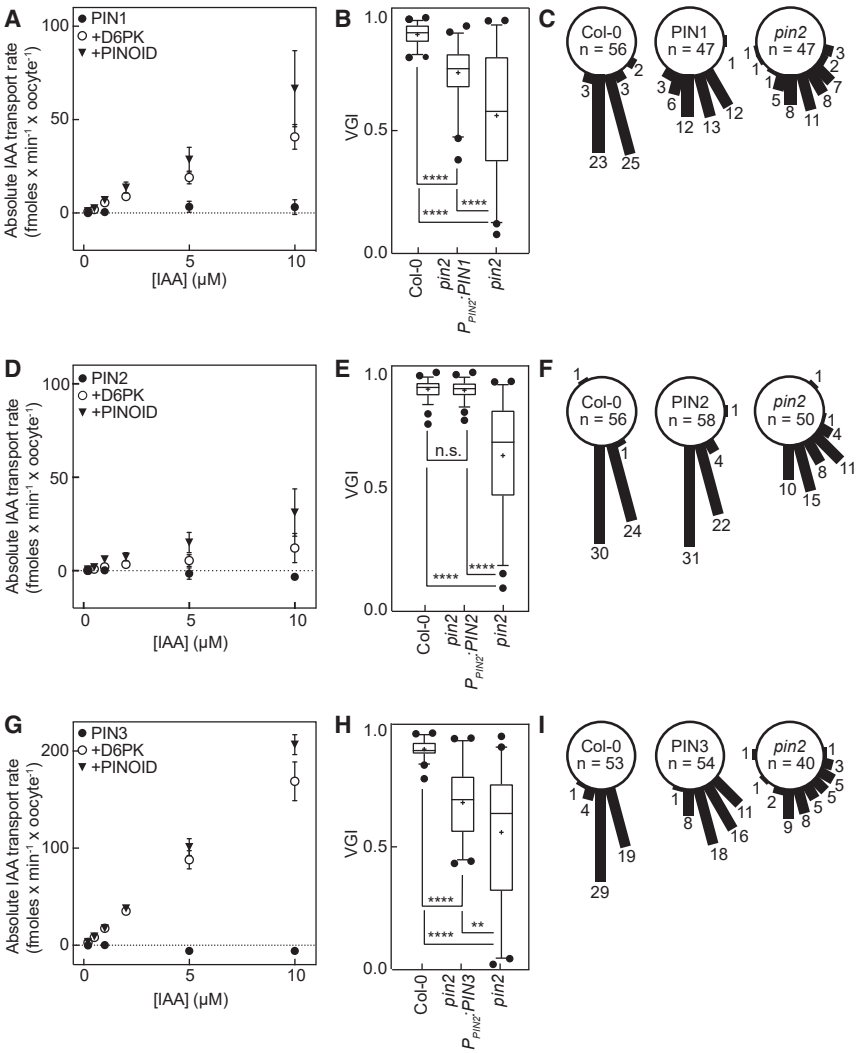

Figure 2. IAA transport properties of canonical PINs in *Xenopus* oocytes and in plants

(A) Transport rates of PIN1 expressed without (●), with D6PK (○), or with PID (▼) as a function of $[IAA]_{in}$.

(B) VGI of a representative T3 P_{PIN2}:*PIN1* line.

(C) Root angles between root tip and gravity vector of a representative homozygous T3 line of PIN1.

(D) Transport rates of PIN2 expressed without (●), with D6PK (○), or with PID (▼) as a function of $[IAA]_{in}$.

(E) VGI of a representative T3 P_{PIN2}:*PIN2* line.

(F) Root angles between root tip and gravity vector of a representative homozygous T3 line of PIN2.

(G) Transport rates of PIN3 expressed without (●), with D6PK (○), or with PID (▼) as a function of $[IAA]_{in}$.

(H) VGI of a representative T3 P_{PIN2}:*PIN3* line.

(I) Root angles between root tip and gravity vector of a representative homozygous T3 line of PIN3. Boxplots range from the 25th to 75th percentiles, whiskers mark the 5th and 95th percentiles, and the median is shown; the mean is represented by (+); points below and above the whiskers are individual points. Data points are mean and SE. Details on statistics and sample sizes are shown in Table S2.

Impact of IAA efflux rates on IAA levels in the root and on root growth

Root gravitropic growth depends on *PIN2* in a growth condition-dependent fashion.[13,20,33] To understand whether the differential transport properties observed in the oocyte system impact gravitropic root growth, we expressed *PIN1*, *PIN2*, and *PIN3* under control of a *PIN2* promoter fragment in the *pin2* mutant. Since both kinases are expressed in the *PIN2* expression domain, and the *pidwag1wag2* mutant also shows agravitropic root growth, it is reasonable to assume that the kinases used in the oocyte system also play a role *in planta* and that the transport rates can be used as a proxy to estimate transport rates in roots.[24,31] We scored the potential of the different PINs to complement the *pin2* agravitropic root growth by screening the root angles of 10 independent lines and isolated a representative line (Figures S2A–S2C). In the homozygous T3 progenies of the representative lines, we compared their vertical growth index (VGI), which considers root length and growth angle of a root, with that of the wild-type Col-0 and *pin2* mutants.[34] We found that, as expected, PIN2 complemented the phenotype to wild-type levels, whereas *PIN1* and *PIN3* complemented the phenotype only partially (Figures 2B, 2C, 2E, 2F, 2H, and 2I).

Next, we investigated the localization of the PINs in root epidermis cells. PIN2 localizes apically in root epidermis cells. This has been suggested to be crucial for proper gravitropic growth.[20,35,36] We determined the polarity index of eight epidermal cells of each PIN-GFP line (Figures 3A and S2D–S2F). We additionally performed immunolocalizations of the wild-type or hemagglutinin (HA)-tagged proteins in epidermal cells (Figure S2G). Consistent with previous studies, PIN2 displayed the highest degree of apical polarity in epidermal cells, whereas PIN1-GFP and PIN3-GFP localized apolarly (Figures 3A and S2G).[20,35,37] The immunolocalizations revealed that PIN1 localized apolarly but predominantly basally, whereas PIN3 localized apolarly but with a preference for the apical membrane (Figure S2G).

We then investigated the IAA response in roots of the different *pin2,* P_{PIN2}:*PIN* lines (Figures 3B–3F). To this end, we transformed these lines with the auxin sensor R2D2, which gives a ratiometric readout of auxin response in a cell that is commonly used as a proxy for auxin levels.[38] We compared the fluorescence ratio in the cortex and epidermis cell files at positions close to the quiescent center (Q) and the transition zone (T). Consistent with previous studies, we found that Col-0 seedlings had low auxin response in the cortex at both positions and low auxin levels in Q, but they had high auxin response at the T position in the epidermis.[39] In contrast, *pin2* mutants displayed a low IAA response in Q and a significantly higher IAA response in T in the cortex, while in the epidermis, the IAA response in

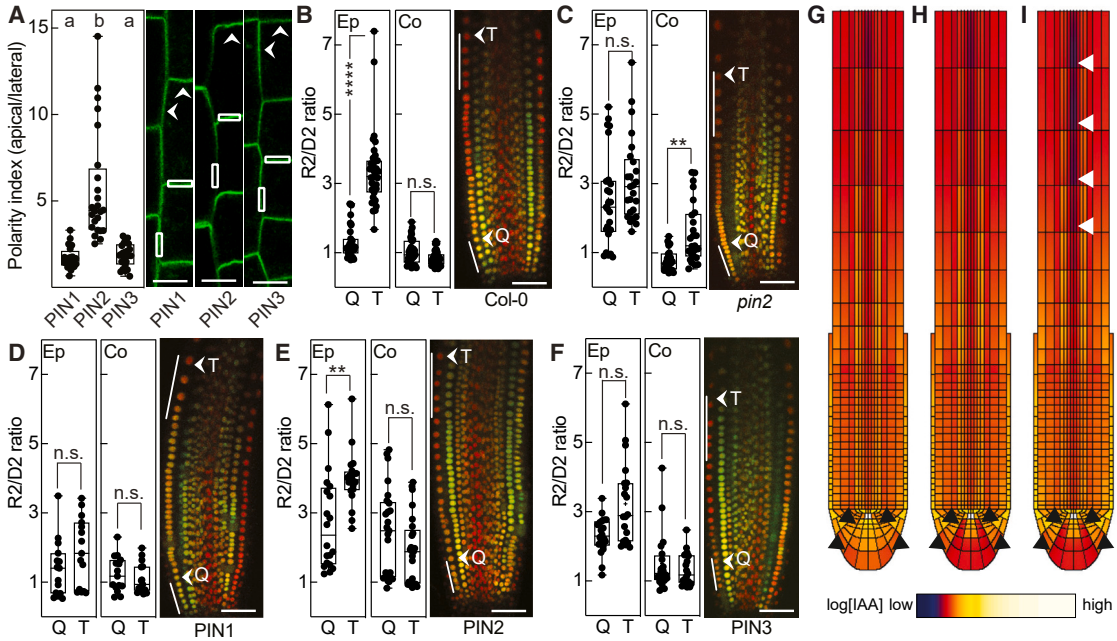

Figure 3. Localization of PINs and IAA response in root tips

(A) Polarity indices of P_{PIN2}:*PIN1-GFP*, P_{PIN2}:*PIN2-GFP*, and P_{PIN2}:*PIN3-GFP* in epidermal cells at the onset of elongation in *pin2*. Representative regions of interest (ROIs) are indicated by white boxes. Mean intensities of ROIs at the apical and the lateral side of the cells were used to calculate the ratios. Arrows indicate the predominant localization. Scale bars represent 10 μm. Boxplots range from the 25th to 75th percentiles, whiskers mark the minimum and maximum values, and the median is shown. Groups were compared by one-way ANOVA, followed by Tukey's post hoc test.

(B–F) Ratio of mDII to DII signal in epidermis (Ep) and cortex (Co). (B) Col-0. (C) *pin2*. (D) P_{PIN2}:*PIN1-GFP* in *pin2*. (E) P_{PIN2}:*PIN2-GFP* in *pin2*. (F) P_{PIN2}:*PIN3-GFP* in *pin2*. The cells indicated by white lines are the first five epidermal cells after anticlinal division of the epidermal/LRC (lateral root cap) initial cell (Q) and five cells at the transition zone as specified by cell elongation (T), which were measured for individual roots. Picture shows overlay of DII (green) and mDII (red) signal. Scale bars represent 40 μm. Boxplots range from the 25th to 75th percentiles, whiskers mark the minimum and maximum values, and the median is shown. Whole dataset analyzed by one-way ANOVA, followed by Tukey's post hoc test.

(G–I) Model auxin distribution patterns. The columella is highlighted by black arrowheads. (G) Simulated auxin pattern for all PINs with equal transport rates. (H) Simulated auxin pattern for 8 times faster transport rates for columella-localized PINs, representing the local presence of faster transporting PIN3. (I) Simulated auxin pattern for 8 times faster transport rates in the columella and 2 times faster transport rates in the vasculature (white arrowheads), representing columella-localized fastest transporting PIN3 and vasculature-localized intermediate fast transporting PIN1. Data points are mean and SE. Details on statistics are shown in Table S2.

Q was higher, thus abolishing a gradient between Q and T. As expected, the IAA response in both cell files of *pin2* P_{PIN2}:*PIN2* lines matched the pattern observed for wild-type plants. For both PIN1 and PIN3, we found no differences between Q and T in either cell file, resulting in an intermediate scenario between the *pin2* mutant and the wild type.

Taken together, we find that all canonical PINs complement the agravitropic defects of the *pin2* mutant, albeit to different degrees. Despite their apolar localization, PIN1 and PIN3 could partially complement the *pin2* mutant's VGI and auxin levels in the relevant cell files. This indicates that PINs have the potential to act partially redundant, but PIN1 seems to possess properties more similar to PIN2 than it is the case for PIN3. This supports the idea that in addition to localization, the transport rates, which are comparatively low in both PIN1 and PIN2, compared with PIN3, are a critical factor.

Different transport rates cause different IAA levels in root cells

To support the idea that transport rates affect IAA levels, we modeled IAA distribution in the root tip (Figures 3G–3I). PIN1, PIN2, and PIN3 act in concert in the *Arabidopsis* root and form a characteristic auxin maximum around the quiescent center.[10,40] The concerted activity of these PINs has been modeled in various studies, always under the assumption that all PINs have equal transport rates, and all these models predicted a strong auxin accumulation in the columella.[41–43] This disagrees with the experimentally determined auxin distribution in root cells that found the columella to be relatively free of IAA.[29] We used our experimentally determined transport parameters and compared the resulting reparametrized model to the existing model that assumes equal transport rates for all PINs (Figures 3G–3I). We found that using the experimentally determined transport rates, the predicted IAA levels in the columella were considerably decreased, and that for this result, particularly, the higher PIN3 transport rate acting in the columella is essential. This shows that the different transport rates we determined *in vitro* can be used to refine models in order to enhance their predictive power.

Investigating the influence of the loop on PIN transport properties

It is well established that the loop of the canonical PINs critically determines their localization in the cell.[35,36,44] It was also

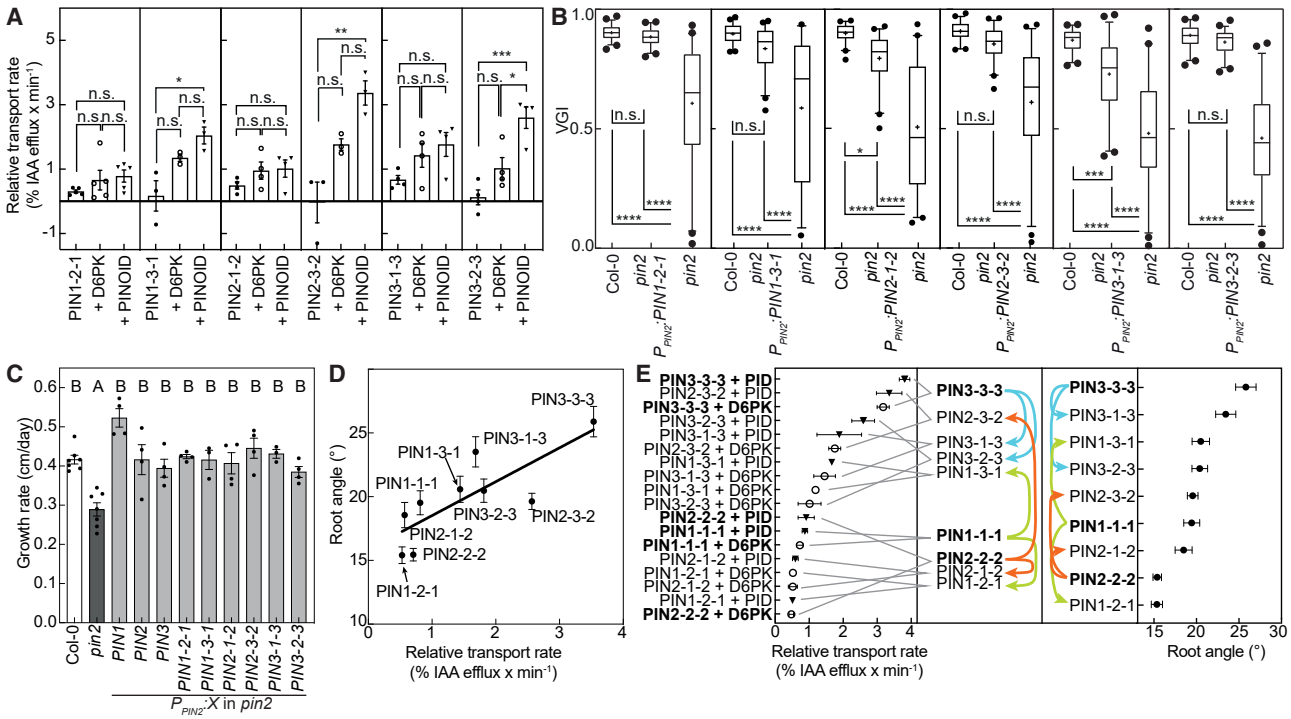

Figure 4. Canonical PIN chimeras are functional IAA transporters whose properties depend on transmembrane and loop donor

(A) Relative IAA export rates for PIN chimeras expressed alone (●) or co-expressed with D6PK (○) or PINOID (▼) in oocytes. Groups were compared by one-way ANOVA, followed by Tukey's post hoc test.

(B) VGIs of the homozygous T3 lines compared with wild type and mutant. Boxplots range from 25th to 75th percentiles, whiskers mark the 5th and 95th percentiles, and the median is indicated. Points below and above the whiskers are drawn as individual points. The mean is indicated by (+). Groups were compared by one-way ANOVA, followed by Dunnett's post hoc test.

(C) Growth rate of homozygous T3 line roots compared with wild-type and *pin2* roots.

(D) Correlation (r = 0.8) between transport rates in oocytes and root angle of the complementing lines.

(E) Chimeras ranked by transport rate (left side) and root angles (right side) of the segregating T2 lines. PIN1 transmembrane domain chimeras are represented by green arrows, PIN2 transmembrane domain chimeras are represented by orange arrows, and PIN3 transmembrane domain chimeras are represented by blue arrows. Data points are mean and SE. Details on statistics are shown in Table S2.

suggested that the loop and the transmembrane domains of PINs coevolved to exert their biological function.[35] To investigate if the loop domain also contributes to the transport properties of PINs, we swapped the loops and the transmembrane domains between PIN1, PIN2, and PIN3 to generate chimeras, e.g., the PIN1-2-1 chimera has the PIN1 transmembrane domains and the PIN2 loop (Figure S3A). We determined the transport rates for the chimeras without kinase or with D6PK or PID at an internal IAA concentration of 1 μM and found that all chimeras mediated IAA efflux from oocytes (Figure 4A). Consistent with the observations for the wild-type proteins, none of the chimeras mediated IAA transport in the absence of kinase, and like the wild-type proteins, all chimeras displayed higher transport rates upon co-expression with PID than with D6PK. Chimera between PIN1 and PIN2 displayed low transport rates. Transport rates of the chimera between PIN1 and PIN3 were intermediate between PIN1 and PIN3. Transport rates were further increased in the chimera between PIN2 and PIN3. In both the PIN1 and the PIN2 transmembrane context, the introduction of the PIN3 loop increased transport rates above the rates observed for the wild-type protein. This surprising result indicates that the loop and the transmembrane domains together define the transport rates of PINs.

To investigate the localization of the chimera *in planta*, we generated GFP-tagged versions of the chimera (Figures S3B–S3G and S4). We successfully recovered a GFP-tagged line for all chimeras except for PIN2-1-2, despite several attempts. All other GFP-tagged chimeras were similar to the untagged versions with respect to the complementation of the mutant phenotypes. We found that the chimera between PIN1 and PIN3 localized apolarly, whereas chimeras containing PIN2 features localized preferentially apically in epidermis cells (Figures S3B–S3G). We next investigated the effect on IAA response in these lines and found that in most instances, the wild-type situation was restored, or at least a situation between wild type and mutant was reached. This indicated that the chimeras have features of the individual domain donors that impact auxin distribution.

We next tested if the transport rates derived for the chimeras in oocytes are reflected *in planta* and investigated their potential to complement the VGI of the *pin2* mutant (Figure 4B). We found that all chimeras complemented the mutant VGI well. Four of the six chimeras were indistinguishable from the wild type; only the VGI of chimeras containing the PIN1 loop were different. Since the VGI depends on root length and root angle, we

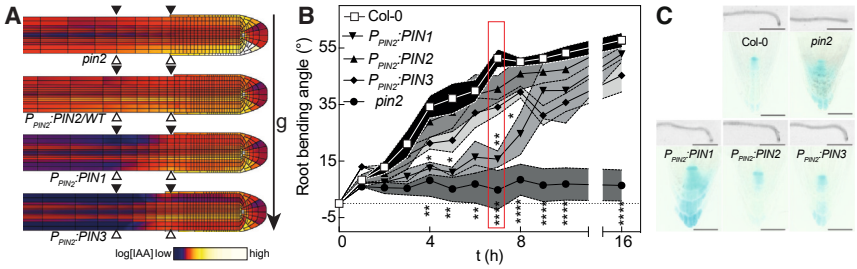

Figure 5. Response of PIN1, PIN2, and PIN3 to a gravitropic stimulus

(A) Model auxin distribution patterns for the genotypes indicated. Simulated auxin pattern for 8 times faster transport rates in the columella and 2 times faster transport rates in the vasculature, representing columella-localized fastest transporting PIN3 and vasculature-localized intermediate fast transporting PIN1. The elongation zone is indicated by black arrowheads (upper side) and white arrowheads (lower side). The gravity vector is indicated.

(B) Root bending kinetics of Col-0, *pin2*, P_{PIN2}*:PIN1*, P_{PIN2}*:PIN2*, and P_{PIN2}*:PIN3* on 0.5 MS medium. Red box highlights the 7-h time point. Data points are mean and SE.

(C) Upper: representative roots of Col-0, the *pin2* mutant, P_{PIN2}*:PIN1*, P_{PIN2}*:PIN2*, and P_{PIN2}*:PIN3* in *pin2* 7 h after the gravitropic stimulus on 0.5 MS medium. Scale bars represent 1 mm. Lower: root tips of the respective genotypes crossed with auxin response reporter Pro_{DR5rev}*:GUS*, stained 7 h after the gravitropic stimulus. Scale bars represent 50 μm. Groups were compared by one-way ANOVA, followed by Dunnett's post hoc test with Col-0 as control group. Data points are mean and SE. Details on statistics are shown in Table S2.

investigated both parameters independently (Figures 4C–4E). It is known that the *pin2* mutant shows a reduced root growth rate.[45] We found that all wild-type PINs and chimeras complemented the growth rate defect, suggesting that the difference in VGI is due to the root angle (Figure 4C). Indeed, we found that the transport rate and root angle correlate strongly (r = 0.8) (Figure 4D). We next ranked the transport rates derived in the oocytes system and the root angle we observed in the representative complementing line (Figure 4E). This clearly illustrates that the root angle critically depends on the transport rate, and as in the case of the wild-type proteins, lower transport rates in the PIN2 expression domain led to more gravitropic root growth than higher transport rates. This is best exemplified in the PIN1-2-1 and PIN2-1-2 chimeras that have similar transport rates to each other as well as wild-type PIN2 and complement the mutant, whereas the PIN2-3-2 and PIN3-2-3 chimeras that have similar transport rates to each other but higher transport rates than PIN2 complement the phenotype to a lesser degree (Figure 4E).

Effect of the transport rates on the response to a gravitropic stimulus

So far, we have investigated how the different transport rates of the individual PINs affect gravitropic root growth. To test if the different transport rates also lead to differences in the response to a gravitropic stimulus, we modeled the expected IAA distribution under this condition (Figure 5A). For the *pin2* mutant, the model predicted strong IAA accumulation in the root meristem with a limited auxin asymmetry in the elongation zone, particularly evident for the vasculature, consistent with this being insufficient to drive root bending.[20] In contrast, for the wild type, the model predicted a significant IAA asymmetry in the elongation zone of the root (Figure 5A, arrowheads), with clear elevation in epidermal and vascular auxin levels at the lower side of the root consistent with experimental observations and leading to well-established root bending.[20,46,47] The model predicted lower IAA levels as well as a decreased elongation zone IAA asymmetry between the upper and lower side of gravistimulated roots for *PIN1* expressed in the *PIN2* domain and even further reduced IAA levels and asymmetry for *PIN3* expressed in the *PIN2* domain, as compared with the wild-type situation (Figure 5A, arrowheads). Based on these auxin patterns, a decreased response to the gravitropic stimulus is expected. To test this prediction experimentally, we turned the plates by 90° and monitored the response in the dark for 16-h plates with sucrose and showed that *pin2* roots failed to reorient to the gravitropic vector (Figure 5B).[20,48] In line with the prediction, we confirmed that roots expressing *PIN1* in the *PIN2* domain showed the expected delayed response to the stimulus, but the root had completely turned after 16 h. Roots expressing *PIN3* in the *PIN2* domain showed an even more delayed response and had not fully adjusted to the gravity vector after 16 h. Consistent with previously published data, *PIN2* complemented the mutant to wild-type levels.[20,48] To test the transcriptional response to IAA in the root tips, we introgressed the P_{DR5}*:GUS* construct into the representative *pin2*, P_{PIN2}*:PIN* lines 7 h after the gravitropic stimulus. Wild-type and P_{PIN2}*:PIN2* plants showed low DR5 response in the quiescent center and columella, whereas P_{PIN2}*:PIN1* and P_{PIN2}*:PIN3* plants displayed high DR5 response in these tissues, as did the *pin2* mutant (Figure 5C). This indicates that also in this regard, PIN1 and PIN3 are similar to each other but different from the wild type as well as the mutant conditions. Finally, we tested the response of the chimera to the gravitropic stimulus. In order to see more subtle differences, we performed these experiments on plates containing sucrose to sustain root growth in the dark, as had been suggested recently (Figure S5).[49,50] In all cases, we observed that the *pin2* mutant displayed negative gravitropic growth following the gravitropic stimulus, consistent with previous observations under these conditions (Figures 5A–5D).[51] We found that all chimera containing PIN2 transmembrane domain or loop domain also complemented this aspect of the *pin2* mutant phenotype fully.

Probing the contribution of the loop to the transport properties of PINs by generating a "pseudo-canonical" PIN

The data we obtained so far prompted us to investigate if features found in the loop can also be transferred to a non-canonical PIN. PIN8 is constitutively active and possesses a short loop but is closely related to PIN3, PIN4, and PIN7, suggesting that PIN8 lost the loop during evolution.[16,52] We therefore introduced the PIN2 or the PIN3 loop between amino acid position 163 and 164 of PIN8 and investigated the biochemical and physiological features of these chimeras.

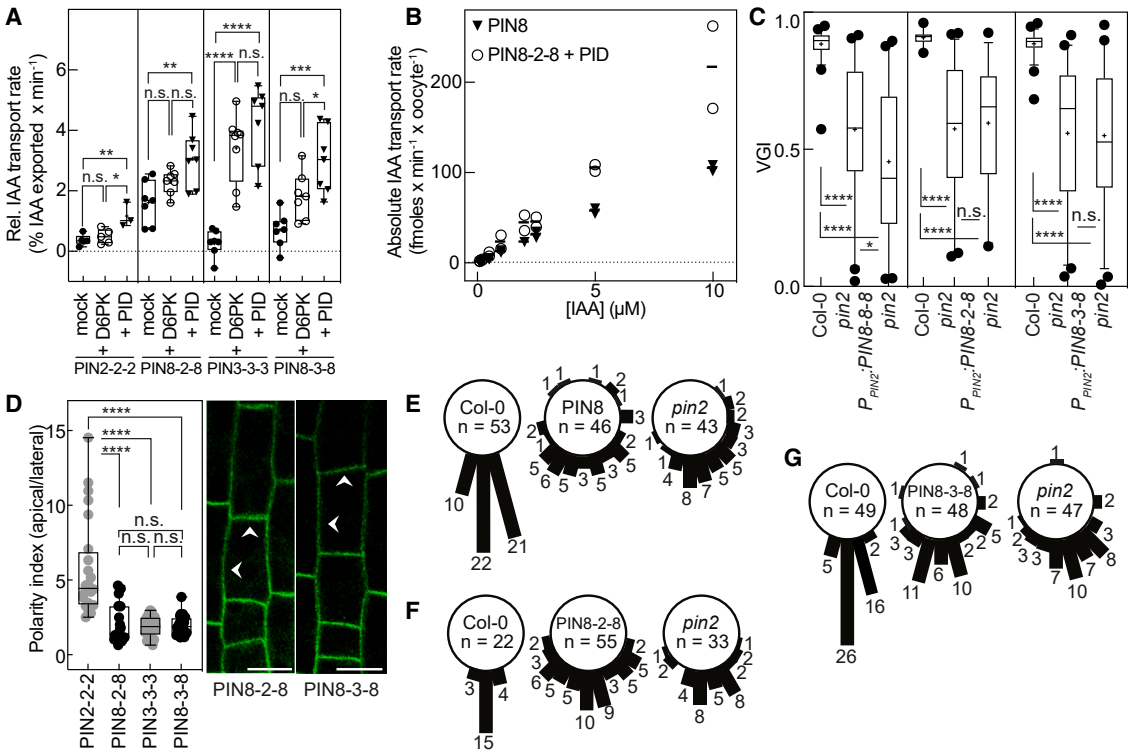

Figure 6. IAA transport properties, localization, and potential to rescue the *pin2* phenotype by PIN8 and pseudo-canonical chimeras

(A) Relative IAA transport rates of PIN2, PIN8-2-8, PIN3, and PIN8-3-8 expressed alone (●) or co-expressed with D6PK (○) or PINOID (▼) in oocytes. Data points are biological replicates using oocytes from different females. Groups were compared by one-way ANOVA, followed by Tukey's post hoc test.

(B) Transport rates as function of $[IAA]_{in}$.

(C) VGIs of a representative homozygous T3 line of P_{PIN2}:*PIN8*, P_{PIN2}:*PIN8-2-8*, and P_{PIN2}:*PIN8-3-8* in *pin2* in comparison to wild type and mutant. Boxplots range from 25th to 75th percentiles, whiskers mark the 5th and 95th percentiles, and the median is indicated. Points below and above the whiskers are drawn as individual points. The mean is indicated by (+). Groups were compared by one-way ANOVA, followed by Tukey's post hoc test.

(D) Polarity indices of PIN8-2-8-GFP and PIN8-3-8-GFP expressed from a *PIN2* promoter fragment in epidermal cells at the onset of elongation in *pin2*. PIN2 and PIN3 were included for comparison as presented in Figure 2. Mean intensities of ROIs at the apical and the lateral side of the cells were used to calculate the ratios. The arrows mark predominant localization. Scale bars represent 10 µm. Boxplots range from 25th to 75th percentiles, whiskers mark the minimum and maximum values, and the median is indicated. Groups were compared by one-way ANOVA, followed by Tukey's post hoc test.

(E–G) Root angles between root tip and gravity vector of a representative homozygous T3 line of P_{PIN2}:*PIN8*, P_{PIN2}:*PIN8-2-8*, and P_{PIN2}:*PIN8-3-8* in the *pin2* mutant background in comparison to wild type and mutant. Numbers represent individual seedlings. Data points are mean and SE. Details on statistics are shown in Table S2.

We found that the PIN8-2-8 and PIN8-3-8 chimeras were functional in the *Xenopus* oocyte assay and mediated N-1-naphthylphthalamic acid (NPA)-sensitive IAA export, indicating that the chimeras display all expected properties of PINs (Figures 6A and S6A).[16,19] Interestingly, we found that the PIN8-2-8 chimera, like PIN8, displayed constitutive IAA transport in the absence of a kinase, whereas the PIN8-3-8 chimera, like a "typical" canonical PIN, does not transport IAA without kinase activation (Figure 6A). In both cases, the introduction of the loop led to an increase of the transport rate upon co-expression with a kinase. Surprisingly, the PIN8-2-8 chimera, upon co-expression of PID, mediated significantly higher IAA export than either PIN2 or PIN8, almost reaching the level of PIN3 (Figures 6A and 6B compared with Figures 1B, 1C, 1E, and 1F). We next investigated the transport rates of PIN8 and the PIN8-2-8 chimera as a function of substrate concentration (Figure 6B). We were able to fit a Michaelis-Menten model to PIN8 with a K_m of 40 µM (Table S1). As was the case for the canonical PINs, we found that for the PID-activated PIN8-2-8, chimera transport rates increased, and we were unable to fit a Michaelis-Menten model, indicating that the chimera displays a lower affinity and that the transport rates are in the seemingly linear range, far below K_m. The PIN8-3-8 chimera exhibited transport properties of a typical canonical PIN: it showed no transport in the absence of a kinase, and it could be activated by kinase co-expression; so, all features of the PIN8-3-8 chimera were almost identical to those of PIN3 (Figure 6A).

We next tested the potential of the pseudo-canonical PINs to complement the VGI of the *pin2* mutant expressed by the chimeras under the control of the *PIN2* promoter fragment and scored the VGI (Figure 6C). We found that the chimeras localized non-polarly to the plasma membrane. Despite the localization to the plasma membrane, the chimeras, as well as PIN8, failed to complement all aspects of the mutant phenotype (Figures 6D–6G and S6B–S6G). This indicates that the potential to IAA transport is not sufficient for a

biological function and supports the hypothesis that the loop and transmembrane domains together are required for PIN function.

DISCUSSION

PINs have different transport properties

We established that canonical PINs have different transport rates that are linear in the IAA concentration range between 0.1 and 10 μM. For technical reasons such as injection volume, substrate concentration, and diffusion from the injection pipette, it is impossible to increase substrate concentration in the oocyte system further, but the observation is consistent with the extremely low substrate affinities established independently for PIN1, PIN3, and PIN8, using isothermal titration calorimetry (ITC), SPR, or solid supported membrane (SSM) electrophysiology, respectively.[15–17] This supports the hypothesis that PINs possess substrate affinities that are much higher than the physiological IAA concentrations.[16] This is a surprising and unexpected finding. One explanation is that when there is abundant auxin, cellular concentration mechanisms increase cytoplasmic concentrations into the mid-micromolar range, which will be well within the working dynamic of PINs. Additionally, if PINs had low micromolar affinities for IAA, they would deprive cells of necessary auxin. Finally, we assumed the IAA concentration range between 0.1 and 10 μM to be physiological based on a hallmark study.[29] We have no reliable information about IAA concentrations in subcellular compartments, but considering that the vacuole occupies up to 90% of the cell volume, cytosolic IAA concentrations may be much higher than we assume.[53] Clearly, this point needs further investigation, but the data available so far point to the conclusion that within the low micromolar range, PINs show a linear correlation between substrate concentration and transport rate. As a consequence, the amount of active transporter in the membrane becomes a critical factor that determines IAA efflux from cells, and clearly, plasma membrane occupancy is tightly controlled by multiple mechanisms.[25,54] The interaction of PINs with kinases is a fast mechanism of activity control and deserves further attention, since canonical PINs do not only display distinct and specific transport properties, but also that these are subject to modification in a kinase-dependent fashion. It is reasonable to assume that the interaction between the transporter and the kinase impacts the structure of the transporter, thus leading to the observed differences in the kinetics. It remains to be investigated how the interaction between PINs and kinases impacts the transport process in a way that can explain the different transport properties despite the similar phosphorylation we observe. A stable heteromer during the transport cycle between transporter and kinase is an intriguing possibility by which the biochemical properties of a transporter can be modified through physical interaction with a regulating kinase.

The IAA flux rate through the epidermis directly depends on the transport rate, which, in addition to the proper PIN localization and flux orientation, is critical for gravitropic root growth since low transport rates ensure that IAA is present long enough in the cell to exert its function. This is also consistent with the conclusion that in addition to proper localization, a low transport rate in the epidermal cell file is required for gravitropic root growth and with the idea that the PIN2 gradient observed after a gravitropic stimulus dampens the IAA gradient and keeps it from becoming too steep.[47] This is reminiscent of the situation in the protophloem, where IAA fluxes must be precisely modulated by the (PROTEIN KINASE ASSOCIATED WITH BRX) PAX/BRX (BREVIS RADIX) rheostat module and where the efflux rate is critical for cell differentiation.[55,56]

The role of the loop in transport

We find that PIN1 and PIN2 are very similar in terms of their biochemical transport properties and their potential to complement the *pin2* mutant phenotypes, while differing in polar localization. The phylogenetically more distantly related PIN3 exhibits a higher transport rate, and its potential to complement the *pin2* mutant phenotypes is lower than that of PIN1 and PIN2. This is partly due to the localization of the transporters that is clearly correlated with the PIN2 loop, as indicated by the localization of the PIN1-2-1 and PIN3-2-3 chimeras (Figures S3B and S3G). This is consistent with previous studies that showed that the *Arabidopsis* PIN2 loop is sufficient to provide positional cues for *Arabidopsis* PINs and for other family members in vascular plants.[35,36] However, additional features must be associated with the PIN2 transmembrane domain as well as the PIN2-3-2 mutant localized apically. Nevertheless, the degree of complementation is, like in the case of wild-type proteins, not strictly correlated with polarity as other chimeras, e.g., PIN1-3-1, also complemented the mutant phenotype to wild-type levels.

We also provided strong evidence that the loop, together with the transmembrane context, contributes to transport. We hypothesize that the activated loop, possibly due to the increased flexibility between the scaffold and the transport domain, increases the transport rate by promoting the flip-back from the outward open to the inward open configuration, the rate-limiting step of the transport cycle.[16] The observation that the PIN3 loop could autoinhibit the PIN8-3-8 chimera, whereas the PIN2 loop in the PIN8-2-8 chimera was unable to do so, is consistent with a previous study that suggests that the transmembrane domains and the loop coevolved and that PIN3 and PIN8 are more closely phylogenetically related, and the autoinhibitory interaction is therefore still possible.[16,35,36,52] This indicates that the interplay of the transmembrane domains and the loop *in planta* is more complex and goes beyond localization to mediate the flux rates required for proper physiological function. How this collaboration works on a mechanistic level and whether the subtle kinase-dependent differences we observed in the transport assays have a role in this process, which translate into physiological differences, remain to be answered in future studies.

Limitations of the study

Even though the biochemical properties of most transporters from plants were obtained in heterologous expression such as yeast and *Xenopus* oocytes systems and yielded robust and reliable results, it is indisputable that the lipid environment of heterologous expression systems is different from the native

environment of these transporters in plants. Therefore, the transport parameters determined in oocytes may differ from the situation *in vivo*, but the unexpectedly high substrate affinity is in line with the parameters determined independently by other labs using different experimental approaches.[15,17] This is also true for the kinase-dependent phosphorylation pattern in oocytes that may not reflect the kinase specificity *in vivo*. Other unknown kinases may also influence the overall phosphorylation of PINs *in planta*, and phosphatases will also counteract it. All these plant-specific enzyme activities are absent from oocytes, and their possible interaction with PINs and influence on IAA transport remain to be explored.

RESOURCE AVAILABILITY

Lead contact

Further information and requests for resources and reagents should be directed to and will be fulfilled by the lead contact, Dr. Ulrich Hammes (ulrich.hammes@tum.de).

Materials availability

Plasmids and transgenic materials generated in this study are available upon request. All data generated in this study are included in the main text or the supplemental information.

Data and code availability

- The mass spectrometry proteomics data have been deposited to the ProteomeXchange Consortium via the PRIDE partner repository with the dataset identifier PXD044850 (user name: reviewer_pxd044850@ebi.ac.uk, password: 3xBdgLSX).[59]
- This paper does not report original codes.
- Any additional information required to reanalyze the data reported in this paper is available from the lead contact upon request.

ACKNOWLEDGMENTS

This work was funded by DFG3468/6-1, DFG3468/6-3, and SFB924 to U.Z.H. We thank Angela Alkofer and Helene Prunkl for excellent technical assistance and *Xenopus* maintenance. Christian Luschnig is acknowledged for sharing unpublished results and valuable discussions.

AUTHOR CONTRIBUTIONS

U.Z.H. conceived and designed the project. D.P.J., L.S., M.K., M.G., K.t.T., J.M., and U.Z.H. conducted research designed together with J.F., C.S., B.K., and K.t.T. J.F., C.S., B.K., and U.Z.H. supervised research. U.Z.H. wrote the manuscript with input from all authors.

DECLARATION OF INTERESTS

The authors declare no competing interests.

STAR★METHODS

Detailed methods are provided in the online version of this paper and include the following:

SUPPLEMENTAL INFORMATION

Supplemental information can be found online at https://doi.org/10.1016/j.devcel.2024.09.020.

Received: October 2, 2023
Revised: June 6, 2024
Accepted: September 18, 2024
Published: October 15, 2024

REFERENCES

1. Benková, E., Michniewicz, M., Sauer, M., Teichmann, T., Seifertová, D., Jürgens, G., and Friml, J. (2003). Local, efflux-dependent auxin gradients as a common module for plant organ formation. Cell *115*, 591–602. https://doi.org/10.1016/s0092-8674(03)00924-3.
2. Han, H., Adamowski, M., Qi, L., Alotaibi, S.S., and Friml, J. (2021). PIN-mediated polar auxin transport regulations in plant tropic responses. New Phytol. *232*, 510–522. https://doi.org/10.1111/nph.17617.
3. Li, L., Gallei, M., and Friml, J. (2022). Bending to auxin: fast acid growth for tropisms. Trends Plant Sci. *27*, 440–449. https://doi.org/10.1016/j.tplants.2021.11.006.
4. Shi, B., and Vernoux, T. (2019). Chapter Four. Patterning at the shoot apical meristem and phyllotaxis. In Current Topics in Developmental Biology, U. Grossniklaus, ed. (Academic Press), pp. 81–107. https://doi.org/10.1016/bs.ctdb.2018.10.003.
5. van den Berg, T., Yalamanchili, K., de Gernier, H., Santos Teixeira, J., Beeckman, T., Scheres, B., Willemsen, V., and ten Tusscher, K. (2021). A reflux-and-growth mechanism explains oscillatory patterning of lateral root branching sites. Dev. Cell *56*, 2176–2191.e10. https://doi.org/10.1016/j.devcel.2021.07.005.
6. Verma, S., Attuluri, V.P.S., and Robert, H.S. (2021). An essential function for auxin in embryo development. Cold Spring Harb. Perspect. Biol. *13*, a039966. https://doi.org/10.1101/cshperspect.a039966.
7. Vieten, A., Vanneste, S., Wisniewska, J., Benková, E., Benjamins, R., Beeckman, T., Luschnig, C., and Friml, J. (2005). Functional redundancy of PIN proteins is accompanied by auxin-dependent cross-regulation of PIN expression. Development *132*, 4521–4531. https://doi.org/10.1242/dev.02027.
8. Wang, Y., and Jiao, Y. (2018). Auxin and above-ground meristems. J. Exp. Bot. *69*, 147–154. https://doi.org/10.1093/jxb/erx299.
9. Hammes, U.Z., Murphy, A.S., and Schwechheimer, C. (2022). Auxin transporters — a biochemical view. Cold Spring Harb. Perspect. Biol. *14*, a039875. https://doi.org/10.1101/cshperspect.a039875.
10. Kleine-Vehn, J., and Friml, J. (2008). Polar targeting and endocytic recycling in auxin-dependent plant development. Annu. Rev. Cell Dev. Biol. *24*, 447–473. https://doi.org/10.1146/annurev.cellbio.24.110707.175254.
11. Michniewicz, M., Brewer, P.B., and Friml, J.Í. (2007). Polar auxin transport and asymmetric auxin distribution. Arabidopsis Book *5*, e0108. https://doi.org/10.1199/tab.0108.
12. Gälweiler, L., Guan, C., Müller, A., Wisman, E., Mendgen, K., Yephremov, A., and Palme, K. (1998). Regulation of polar auxin transport by AtPIN1 in Arabidopsis vascular tissue. Science *282*, 2226–2230. https://doi.org/10.1126/science.282.5397.2226.

13. Müller, A., Guan, C., Gälweiler, L., Tänzler, P., Huijser, P., Marchant, A., Parry, G., Bennett, M., Wisman, E., and Palme, K. (1998). AtPIN2 defines a locus of Arabidopsis for root gravitropism control. EMBO J. *17*, 6903–6911. https://doi.org/10.1093/emboj/17.23.6903.

14. Willige, B.C., Ahlers, S., Zourelidou, M., Barbosa, I.C.R., Demarsy, E., Trevisan, M., Davis, P.A., Roelfsema, M.R.G., Hangarter, R., Fankhauser, C., et al. (2013). D6PK AGCVIII kinases are required for auxin transport and phototropic hypocotyl bending in Arabidopsis. Plant Cell *25*, 1674–1688. https://doi.org/10.1105/tpc.113.111484.

15. Su, N., Zhu, A., Tao, X., Ding, Z.J., Chang, S., Ye, F., Zhang, Y., Zhao, C., Chen, Q., Wang, J., et al. (2022). Structures and mechanisms of the Arabidopsis auxin transporter PIN3. Nature *609*, 616–621. https://doi.org/10.1038/s41586-022-05142-w.

16. Ung, K.L., Winkler, M., Schulz, L., Kolb, M., Janacek, D.P., Dedic, E., Stokes, D.L., Hammes, U.Z., and Pedersen, B.P. (2022). Structures and mechanism of the plant PIN-FORMED auxin transporter. Nature *609*, 605–610. https://doi.org/10.1038/s41586-022-04883-y.

17. Yang, Z., Xia, J., Hong, J., Zhang, C., Wei, H., Ying, W., Sun, C., Sun, L., Mao, Y., Gao, Y., et al. (2022). Structural insights into auxin recognition and efflux by Arabidopsis PIN1. Nature *609*, 611–615. https://doi.org/10.1038/s41586-022-05143-9.

18. Ung, K.L., Schulz, L., Stokes, D.L., Hammes, U.Z., and Pedersen, B.P. (2023). Substrate recognition and transport mechanism of the PIN-FORMED auxin exporters. Trends Biochem. Sci. *48*, 937–948. https://doi.org/10.1016/j.tibs.2023.07.006.

19. Abas, L., Kolb, M., Stadlmann, J., Janacek, D.P., Lukic, K., Schwechheimer, C., Sazanov, L.A., Mach, L., Friml, J., and Hammes, U.Z. (2021). Naphthylphthalamic acid associates with and inhibits PIN auxin transporters. Proc. Natl. Acad. Sci. USA *118*, e2020857118. https://doi.org/10.1073/pnas.2020857118.

20. Abas, L., Benjamins, R., Malenica, N., Paciorek, T., Wiśniewska, J., Moulinier-Anzola, J.C., Sieberer, T., Friml, J., and Luschnig, C. (2006). Intracellular trafficking and proteolysis of the Arabidopsis auxin-efflux facilitator PIN2 are involved in root gravitropism. Nat. Cell Biol. *8*, 249–256. https://doi.org/10.1038/ncb1369.

21. Zourelidou, M., Absmanner, B., Weller, B., Barbosa, I.C.R., Willige, B.C., Fastner, A., Streit, V., Port, S.A., Colcombet, J., de la Fuente van Bentem, S., et al. (2014). Auxin efflux by PIN-FORMED proteins is activated by two different protein kinases, D6 PROTEIN kinase and PINOID. eLife *3*, e02860. https://doi.org/10.7554/eLife.02860.

22. Christensen, S.K., Dagenais, N., Chory, J., and Weigel, D. (2000). Regulation of auxin response by the protein kinase PINOID. Cell *100*, 469–478. https://doi.org/10.1016/s0092-8674(00)80682-0.

23. Friml, J., Yang, X., Michniewicz, M., Weijers, D., Quint, A., Tietz, O., Benjamins, R., Ouwerkerk, P.B.F., Ljung, K., Sandberg, G., et al. (2004). A PINOID-dependent binary switch in apical-basal PIN polar targeting directs auxin efflux. Science *306*, 862–865. https://doi.org/10.1126/science.1100618.

24. Zourelidou, M., Müller, I., Willige, B.C., Nill, C., Jikumaru, Y., Li, H., and Schwechheimer, C. (2009). The polarly localized D6 protein kinase is required for efficient auxin transport in *Arabidopsis thaliana*. Development *136*, 627–636. https://doi.org/10.1242/dev.028365.

25. Lanassa Bassukas, A.E.L., Xiao, Y., and Schwechheimer, C. (2022). Phosphorylation control of PIN auxin transporters. Curr. Opin. Plant Biol. *65*, 102146. https://doi.org/10.1016/j.pbi.2021.102146.

26. Salvi, E., Rutten, J.P., Di Mambro, R., Polverari, L., Licursi, V., Negri, R., Dello Ioio, R., Sabatini, S., and Ten Tusscher, K. (2020). A self-organized PLT/Auxin/ARR-B network controls the dynamics of root zonation development in *Arabidopsis thaliana*. Dev. Cell *53*, 431–443.e23. https://doi.org/10.1016/j.devcel.2020.04.004.

27. Barbosa, I.C.R., Hammes, U.Z., and Schwechheimer, C. (2018). Activation and polarity control of PIN-FORMED auxin transporters by phosphorylation. Trends Plant Sci. *23*, 523–538. https://doi.org/10.1016/j.tplants.2018.03.009.

28. Kleine-Vehn, J., Ding, Z., Jones, A.R., Tasaka, M., Morita, M.T., and Friml, J. (2010). Gravity-induced PIN transcytosis for polarization of auxin fluxes in gravity-sensing root cells. Proc. Natl. Acad. Sci. USA *107*, 22344–22349. https://doi.org/10.1073/pnas.1013145107.

29. Petersson, S.V., Johansson, A.I., Kowalczyk, M., Makoveychuk, A., Wang, J.Y., Moritz, T., Grebe, M., Benfey, P.N., Sandberg, G., and Ljung, K. (2009). An auxin gradient and maximum in the Arabidopsis root apex shown by high-resolution cell-specific analysis of IAA distribution and synthesis. Plant Cell *21*, 1659–1668. https://doi.org/10.1105/tpc.109.066480.

30. Mergner, J., Frejno, M., List, M., Papacek, M., Chen, X., Chaudhary, A., Samaras, P., Richter, S., Shikata, H., Messerer, M., et al. (2020). Mass-spectrometry-based draft of the Arabidopsis proteome. Nature *579*, 409–414. https://doi.org/10.1038/s41586-020-2094-2.

31. Dhonukshe, P., Huang, F., Galvan-Ampudia, C.S., Mähönen, A.P., Kleine-Vehn, J., Xu, J., Quint, A., Prasad, K., Friml, J., Scheres, B., et al. (2010). Plasma membrane-bound AGC3 kinases phosphorylate PIN auxin carriers at TPRXS(N/S) motifs to direct apical PIN recycling. Development *137*, 3245–3255. https://doi.org/10.1242/dev.052456.

32. Huang, F., Zago, M.K., Abas, L., van Marion, A., Galván-Ampudia, C.S., and Offringa, R. (2010). Phosphorylation of conserved PIN motifs directs Arabidopsis PIN1 polarity and auxin transport. Plant Cell *22*, 1129–1142. https://doi.org/10.1105/tpc.109.072678.

33. Luschnig, C., Gaxiola, R.A., Grisafi, P., and Fink, G.R. (1998). EIR1, a root-specific protein involved in auxin transport, is required for gravitropism in *Arabidopsis thaliana*. Genes Dev. *12*, 2175–2187. https://doi.org/10.1101/gad.12.14.2175.

34. Grabov, A., Ashley, M.K., Rigas, S., Hatzopoulos, P., Dolan, L., and Vicente-Agullo, F. (2005). Morphometric analysis of root shape. New Phytol. *165*, 641–651. https://doi.org/10.1111/j.1469-8137.2004.01258.x.

35. Zhang, Y., Hartinger, C., Wang, X., and Friml, J. (2020). Directional auxin fluxes in plants by intramolecular domain-domain coevolution of PIN auxin transporters. New Phytol. *227*, 1406–1416. https://doi.org/10.1111/nph.16629.

36. Zhang, Y., Xiao, G., Wang, X., Zhang, X., and Friml, J. (2019). Evolution of fast root gravitropism in seed plants. Nat. Commun. *10*, 3480. https://doi.org/10.1038/s41467-019-11471-8.

37. Michniewicz, M., Zago, M.K., Abas, L., Weijers, D., Schweighofer, A., Meskiene, I., Heisler, M.G., Ohno, C., Zhang, J., Huang, F., et al. (2007). Antagonistic regulation of PIN phosphorylation by PP2A and PINOID directs auxin flux. Cell *130*, 1044–1056. https://doi.org/10.1016/j.cell.2007.07.033.

38. Liao, C.-Y., Smet, W., Brunoud, G., Yoshida, S., Vernoux, T., and Weijers, D. (2015). Reporters for sensitive and quantitative measurement of auxin response. Nat. Methods *12*, 207–210. https://doi.org/10.1038/nmeth.3279.

39. Mellor, N.L., Voß, U., Janes, G., Bennett, M.J., Wells, D.M., and Band, L.R. (2020). Auxin fluxes through plasmodesmata modify root-tip auxin distribution. Development *147*, dev181669. https://doi.org/10.1242/dev.181669.

40. Friml, J., Benková, E., Blilou, I., Wisniewska, J., Hamann, T., Ljung, K., Woody, S., Sandberg, G., Scheres, B., Jürgens, G., et al. (2002). AtPIN4 mediates sink-driven auxin gradients and root patterning in Arabidopsis. Cell *108*, 661–673. https://doi.org/10.1016/s0092-8674(02)00656-6.

41. Band, L.R., Wells, D.M., Fozard, J.A., Ghetiu, T., French, A.P., Pound, M.P., Wilson, M.H., Yu, L., Li, W., Hijazi, H.I., et al. (2014). Systems analysis of auxin transport in the Arabidopsis root apex. Plant Cell *26*, 862–875. https://doi.org/10.1105/tpc.113.119495.

42. Di Mambro, R., De Ruvo, M., Pacifici, E., Salvi, E., Sozzani, R., Benfey, P.N., Busch, W., Novak, O., Ljung, K., Di Paola, L., et al. (2017). Auxin minimum triggers the developmental switch from cell division to cell differentiation in the Arabidopsis root. Proc. Natl. Acad. Sci. USA *114*, E7641–E7649. https://doi.org/10.1073/pnas.1705833114.

43. Grieneisen, V.A., Xu, J., Marée, A.F.M., Hogeweg, P., and Scheres, B. (2007). Auxin transport is sufficient to generate a maximum and gradient guiding root growth. Nature *449*, 1008–1013. https://doi.org/10.1038/nature06215.

44. Ganguly, A., Park, M., Kesawat, M.S., and Cho, H.T. (2014). Functional analysis of the hydrophilic loop in intracellular trafficking of Arabidopsis PIN-FORMED proteins. Plant Cell *26*, 1570–1585. https://doi.org/10.1105/tpc.113.118422.

45. Blilou, I., Xu, J., Wildwater, M., Willemsen, V., Paponov, I., Friml, J., Heidstra, R., Aida, M., Palme, K., and Scheres, B. (2005). The PIN auxin efflux facilitator network controls growth and patterning in Arabidopsis roots. Nature *433*, 39–44. https://doi.org/10.1038/nature03184.

46. Ottenschläger, I., Wolff, P., Wolverton, C., Bhalerao, R.P., Sandberg, G., Ishikawa, H., Evans, M., and Palme, K. (2003). Gravity-regulated differential auxin transport from columella to lateral root cap cells. Proc. Natl. Acad. Sci. USA *100*, 2987–2991. https://doi.org/10.1073/pnas.0437936100.

47. Retzer, K., Akhmanova, M., Konstantinova, N., Malínská, K., Leitner, J., Petrášek, J., and Luschnig, C. (2019). Brassinosteroid signaling delimits root gravitropism via sorting of the Arabidopsis PIN2 auxin transporter. Nat. Commun. *10*, 5516. https://doi.org/10.1038/s41467-019-13543-1.

48. Baster, P., Robert, S., Kleine-Vehn, J., Vanneste, S., Kania, U., Grunewald, W., De Rybel, B., Beeckman, T., and Friml, J. (2013). SCFTIR1/AFB-auxin signalling regulates PIN vacuolar trafficking and auxin fluxes during root gravitropism. EMBO J. *32*, 260–274. https://doi.org/10.1038/emboj.2012.310.

49. García-González, J., Lacek, J., and Retzer, K. (2021). Dissecting hierarchies between light, sugar and auxin action underpinning root and root hair growth. Plants (Basel) *10*, 111. https://doi.org/10.3390/plants10010111.

50. Thomas, M., Soriano, A., O'Connor, C., Crabos, A., Nacry, P., Thompson, M., Hrabak, E., Divol, F., and Péret, B. (2023). *pin2* mutant agravitropic root phenotype is conditional and nutrient-sensitive. Plant Sci. *329*, 111606. https://doi.org/10.1016/j.plantsci.2023.111606.

51. Leitner, J., Petrášek, J., Tomanov, K., Retzer, K., Pařezová, M., Korbei, B., Bachmair, A., Zažímalová, E., and Luschnig, C. (2012). Lysine^{63}-linked ubiquitylation of PIN2 auxin carrier protein governs hormonally controlled adaptation of *Arabidopsis* root growth. Proc. Natl. Acad. Sci. USA *109*, 8322–8327. https://doi.org/10.1073/pnas.1200824109.

52. Bennett, T., Brockington, S.F., Rothfels, C., Graham, S.W., Stevenson, D., Kutchan, T., Rolf, M., Thomas, P., Wong, G.K.S., Leyser, O., et al. (2014). Paralogous radiations of PIN proteins with multiple origins of noncanonical PIN structure. Mol. Biol. Evol. *31*, 2042–2060. https://doi.org/10.1093/molbev/msu147.

53. Krüger, F., and Schumacher, K. (2018). Pumping up the volume – vacuole biogenesis in Arabidopsis thaliana. Semin. Cell Dev. Biol. *80*, 106–112. https://doi.org/10.1016/j.semcdb.2017.07.008.

54. Marhava, P. (2022). Recent developments in the understanding of PIN polarity. New Phytol. *233*, 624–630. https://doi.org/10.1111/nph.17867.

55. Marhava, P., Bassukas, A.E.L., Zourelidou, M., Kolb, M., Moret, B., Fastner, A., Schulze, W.X., Cattaneo, P., Hammes, U.Z., Schwechheimer, C., et al. (2018). A molecular rheostat adjusts auxin flux to promote root protophloem differentiation. Nature *558*, 297–300. https://doi.org/10.1038/s41586-018-0186-z.

56. Moret, B., Marhava, P., Aliaga Fandino, A.C., Hardtke, C.S., and Ten Tusscher, K.H.W. (2020). Local auxin competition explains fragmented differentiation patterns. Nat. Commun. *11*, 2965. https://doi.org/10.1038/s41467-020-16803-7.

57. Lampropoulos, A., Sutikovic, Z., Wenzl, C., Maegele, I., Lohmann, J.U., and Forner, J. (2013). GreenGate - A novel, versatile, and efficient cloning system for plant transgenesis. PLoS One *8*, e83043. https://doi.org/10.1371/journal.pone.0083043.

58. Willige, B.C., Isono, E., Richter, R., Zourelidou, M., and Schwechheimer, C. (2011). Gibberellin regulates PIN-FORMED abundance and is required for auxin transport-dependent growth and development in Arabidopsis thaliana. Plant Cell *23*, 2184–2195. https://doi.org/10.1105/tpc.111.086355.

59. Perez-Riverol, Y., Csordas, A., Bai, J., Bernal-Llinares, M., Hewapathirana, S., Kundu, D.J., Inuganti, A., Griss, J., Mayer, G., Eisenacher, M., et al. (2019). The PRIDE database and related tools and resources in 2019: improving support for quantification data. Nucleic Acids Res. *47*, D442–D450. https://doi.org/10.1093/nar/gky1106.

60. Ludewig, U., von Wirén, N., and Frommer, W.B. (2002). Uniport of NH4+ by the root hair plasma membrane ammonium transporter LeAMT1;1. J. Biol. Chem. *277*, 13548–13555. https://doi.org/10.1074/jbc.M200739200.

61. Fastner, A., Absmanner, B., and Hammes, U.Z. (2017). Use of *Xenopus laevis* oocytes to study auxin transport. Methods Mol. Biol. *1497*, 259–270. https://doi.org/10.1007/978-1-4939-6469-7_21.

62. Bradford, M.M. (1976). A rapid and sensitive method for the quantitation of microgram quantities of protein utilizing the principle of protein-dye binding. Anal. Biochem. *72*, 248–254. https://doi.org/10.1006/abio.1976.9999.

63. Ruprecht, B., Koch, H., Domasinska, P., Frejno, M., Kuster, B., and Lemeer, S. (2017). Optimized enrichment of phosphoproteomes by Fe-IMAC column chromatography. Methods Mol. Biol. *1550*, 47–60. https://doi.org/10.1007/978-1-4939-6747-6_5.

64. Marx, H., Lemeer, S., Schliep, J.E., Matheron, L., Mohammed, S., Cox, J., Mann, M., Heck, A.J.R., and Kuster, B. (2013). A large synthetic peptide and phosphopeptide reference library for mass spectrometry–based proteomics. Nat. Biotechnol. *31*, 557–564. https://doi.org/10.1038/nbt.2585.

65. Zolg, D.P., Wilhelm, M., Yu, P., Knaute, T., Zerweck, J., Wenschuh, H., Reimer, U., Schnatbaum, K., and Kuster, B. (2017). PROCAL: A set of 40 peptide standards for retention time indexing, column performance monitoring, and collision energy calibration. Proteomics *17*, 1700263. https://doi.org/10.1002/pmic.201700263.

66. Hahne, H., Pachl, F., Ruprecht, B., Maier, S.K., Klaeger, S., Helm, D., Médard, G., Wilm, M., Lemeer, S., and Kuster, B. (2013). DMSO enhances electrospray response, boosting sensitivity of proteomic experiments. Nat. Methods *10*, 989–991. https://doi.org/10.1038/nmeth.2610.

67. Tyanova, S., Temu, T., and Cox, J. (2016). The MaxQuant computational platform for mass spectrometry-based shotgun proteomics. Nat. Protoc. *11*, 2301–2319. https://doi.org/10.1038/nprot.2016.136.

68. Cheng, C.-Y., Krishnakumar, V., Chan, A.P., Thibaud-Nissen, F., Schobel, S., and Town, C.D. (2017). Araport11: a complete reannotation of the Arabidopsis thaliana reference genome. Plant J. *89*, 789–804. https://doi.org/10.1111/tpj.13415.

69. Tyanova, S., Temu, T., Sinitcyn, P., Carlson, A., Hein, M.Y., Geiger, T., Mann, M., and Cox, J. (2016). The Perseus computational platform for comprehensive analysis of (prote)omics data. Nat. Methods *13*, 731–740. https://doi.org/10.1038/nmeth.3901.

70. Clough, S.J., and Bent, A.F. (1998). Floral dip: a simplified method for Agrobacterium-mediated transformation of Arabidopsis thaliana. Plant J. *16*, 735–743. https://doi.org/10.1046/j.1365-313x.1998.00343.x.

71. Sauer, M., Paciorek, T., Benková, E., and Friml, J. (2006). Immunocytochemical techniques for whole-mount *in situ* protein localization in plants. Nat. Protoc. *1*, 98–103. https://doi.org/10.1038/nprot.2006.15.

72. Wisniewska, J., Xu, J., Seifertová, D., Brewer, P.B., Ruzicka, K., Blilou, I., Rouquié, D., Benková, E., Scheres, B., and Friml, J. (2006). Polar PIN localization directs auxin flow in plants. Science *312*, 883. https://doi.org/10.1126/science.1121356.

73. Paciorek, T., Zazímalová, E., Ruthardt, N., Petrásek, J., Stierhof, Y.D., Kleine-Vehn, J., Morris, D.A., Emans, N., Jürgens, G., Geldner, N., et al. (2005). Auxin inhibits endocytosis and promotes its own efflux from cells. Nature *435*, 1251–1256. https://doi.org/10.1038/nature03633.

74. Santos Teixeira, J., van den Berg, T., and ten Tusscher, K. (2022). Complementary roles for auxin and auxin signalling revealed by reverse

engineering lateral root stable prebranch site formation. Development *149*, dev200927. https://doi.org/10.1242/dev.200927.

75. Grones, P., Abas, M., Hajný, J., Jones, A., Waidmann, S., Kleine-Vehn, J., and Friml, J. (2018). PID/WAG-mediated phosphorylation of the Arabidopsis PIN3 auxin transporter mediates polarity switches during gravitropism. Sci. Rep. *8*, 10279. https://doi.org/10.1038/s41598-018-28188-1.

76. Arshadi, C., Günther, U., Eddison, M., Harrington, K.I.S., and Ferreira, T.A. (2021). SNT: a unifying toolbox for quantification of neuronal anatomy. Nat. Methods *18*, 374–377. https://doi.org/10.1038/s41592-021-01105-7.

77. Ferreira, T.A., Blackman, A.V., Oyrer, J., Jayabal, S., Chung, A.J., Watt, A.J., Sjöström, P.J., and van Meyel, D.J. (2014). Neuronal morphometry directly from bitmap images. Nat. Methods *11*, 982–984. https://doi.org/10.1038/nmeth.3125.

STAR★METHODS

KEY RESOURCES TABLE

REAGENT or RESOURCE	SOURCE	IDENTIFIER
Bacterial and virus strains		
Agrobacterium tumefaciens GV3101	Widely distributed	N/A
XL1 Blue *E.Coli*	Widely distributed	N/A
Biological samples		
Col-0	https://www.ncbi.nlm.nih.gov/Taxonomy/Browser/wwwtax.cgi	NCBI:txid3702
pin2 mutant	Willige et al.[14]	*SALK_042899.22.25.x*
R2D2	Liao et al.[38]	N/A
Chemicals, peptides, and recombinant proteins		
^{3}H-IAA (25 Ci/mmol, 1 mCi/mmol)	RC Tritec (Teufen, Switzerland)	RCTT1370
PhosSTOP	Roche	4906845001
cOmplete™ EDTA-free proteinase inhibitor cocktail	Sigma-Aldrich	4693132001
Murashige & Skoog medium, including B5 vitamins	Duchefa Farma, Harleem, Netherlands	M0231
All other chemicals were standard lab grade	Sigma-Aldrich or Carl Roth	N/A
Critical commercial assays		
mMESSAGE mMACHINE™ SP6 Transcription kit	Thermo Fisher Scientific	AM1340
MEGAclear Purification of Transcription Reactions kit	Thermo Fisher Scientific	AM1908
Deposited data		
ProteomeXchange	This study	PXD044850
Experimental models: Organisms/strains		
All plant lines	This study	N/A
Oligonucleotides		
Table S3	N/A	N/A
Recombinant DNA		
pOO2	Ludewig et al.[60]	N/A
R2D2	Liao et al.[38]	N/A
Greengate vectors	Lampropoulos et al.[57]	N/A
Software and algorithms		
ImageJ	https://imagej.net/Welcome	N/A
GraphPadPrism 10.2.3	https://www.graphpad.com	N/A

EXPERIMENTAL MODEL AND STUDY PARTICIPANT DETAILS

Plant Materials and Growth Conditions

Arabidopsis thaliana Columbia-0 ecotype was used as the wild type. The *pin2* mutant used in this study was described previously.[58] For growth in pots, the seeds were spread on moist soil and incubated in the growth chamber with a cover under long day conditions (16 h light, 8 h dark, 21-23 °C). After one week, the cover was removed and the plants were separated to individual pots, if necessary. For growth on plates, the seeds were sterilized with chlorine gas (6 %(v/v), 1 h) and homogenously spread on the agar or placed individually with an autoclaved toothpick. Plates were sealed and incubated at 4 °C in the dark for two days. Afterwards the plates were placed vertically in plant growth chambers (Sanyo or Panasonic) under long day conditions (16 h light, 8 h dark, 21 °C, 110 to 130 μmol/m^2 sec; Osram L36W/ 840 Lumilux Cool White Hg).

Solid 0.5 MS medium contained 2.15 g/l Murashige & Skoog medium, including B5 vitamins (Duchefa Farma, Harleem, Netherlands), 0.5 g/l MES monohydrate (Carl Roth, Karlsruhe, Germany) and 0.8 % (w/v) plant agar (Duchefa Farma). Solid Growth medium contained 4.3 g/l MS medium, including B5 vitamins incl. Gamborg B5 vitamins, 0.5 g/l MES monohydrate, 0.7 % (w/v) plant agar and 1 % (w/v) saccharose.

Xenopus laevis females

Wild type *Xenopus laevis* females for oocyte extraction are kept in a licensed facility at TUM according to the relevant animal welfare regulations and all applicable laws.

METHOD DETAILS

Cloning procedures

Plant expression vectors were generated by a modified GreenGate cloning protocol.[57] Primer sequences for cloning are reported in Table S3. The BsaI-recognition site and, if necessary, suitable overhangs were added to the DNA fragments by PCR. The DNA fragments of interest were amplified from genomic DNA or synthesized by Geneart, Thermo Fisher (Regensburg, Germany). The transmembrane and loop domains of PIN1, PIN2, PIN3 and PIN8 were defined according to.[44] PIN1: TM1 1–156 aa, loop 157–459 aa, TM2 460–623 aa. PIN2: TM1 1–156 aa, loop 157–484 aa, TM2 485–623 aa. PIN3: TM1 1–156 aa, loop 157–477 aa, TM2 478–641 aa. PIN8: TM1 1–163 aa, loop 164–204 aa, TM2 205–367 aa. The CDS of eGFP was inserted C-terminally of amino acid positions 432 (PIN1), 301 (PIN2) and 451 (PIN3) or at equivalent positions in the loop domain in the PIN chimeras.[44] The loops of PIN1, PIN2 or PIN3 were inserted C-terminally of position 163 in PIN8.

Xenopus laevis oocyte transport assay

For cloning into pOO2,[60] the coding sequences were amplified with 5′-phosphorylated oligos and purified by gel electrophoreses and sequenced. The efflux experiments were performed as described.[61] For cRNA synthesis, the mMESSAGE mMACHINE™ SP6 Transcription kit and the MEGAclear Purification of Transcription Reactions kit from Thermo Fisher Scientific were used according to the manufacturer's protocol. Oocytes were injected with 50 nL of 150 ng/μl PIN cRNA and 75 ng/μl cRNA of respective kinase. ^{3}H-IAA (25 Ci/mmol, 1 mCi/mmol) was purchased from ARC (Saint Louis, USA) or RC Tritec (Teufen, Switzerland). After four days, oocytes were injected with substrate to reach the desired internal IAA concentration. For each ach time point (0, 5, 10, 15 min for PIN3, PIN2-3-2, PIN3-1-3, PIN3-2-3, PIN8 or 0, 7.5, 15, 30 min for PIN1, PIN2, PIN1-2-1, PIN2-1-2, PIN8-2-8, PIN8-3-8) at least seven oocytes were used. The transport rates for each concentration were calculated by linear regression. Experiments were performed at least three times with oocytes from different *X. laevis* females.

(Phospho)proteomic sample preparation

Oocytes (n = 50) expressing either PIN1, PIN2, PIN3 alone or PIN co-expressed with YFP-D6PK or PINOID were collected without oocyte buffer in a reaction tube (2 ml). The oocytes were homogenized in 2 ml Lysis buffer (Tris-HCl pH 8.0 50 mM, ½ tablet PhosSTOP (Roche), 1x cOmplete™ EDTA-free proteinase inhibitor cocktail (Sigma-Aldrich), 1 % SDC) and centrifuged (2000 *g*, 10 min, 4 °C). The supernatant without yolk was transferred to a reaction tube suitable for ultracentrifugation and centrifuged (150 000 *g*, 30 min, 4 °C). The cytosolic fraction (supernatant) and the membrane fraction (pellet) were split, and the membrane fraction was resuspended in 400 μl Lysis buffer. All samples were stored at –80 °C before preparation for LC-MS/MS analysis.

Proteins were precipitated over night with 10% tricholoroacetic acid in acetone at -20 °C and subsequently washed two times with ice-cold acetone. Dry samples were incubated with urea digestion buffer (8 M urea, 50 mM Tris-HCl pH 8.5, 1 mM DTT, cOmplete™ EDTA-free protease inhibitor cocktail (PIC, Roche, Basel, Switzerland), Phosphatase inhibitor (PI-III; in-house, composition resembling Phosphatase inhibitor cocktail 1,2 and 3 from Sigma-Aldrich, St. Louis, USA) for 1 h. Protein concentration was determined with a Bradford assay.[62] For each sample 20 μg (cytoplasm) or 80 μg (membrane) of protein was reduced (10 mM DTT), alkylated (55 mM chloroacetamide), and diluted 1:5 with digestion buffer (50 mM Tris-HCl pH 8.5, 1 mM $CaCl_2$). In-solution digestion with trypsin (1:100 w/w) at 37 °C was performed in two steps (4 h; overnight). Digested samples were acidified with formic acid (FA) and centrifuged at 14,000 *g* for 15 min at 4 °C. Cytoplasm samples were desalted on self-packed StageTips (three disks, Ø 1.5 mm C18 material, 3M Empore™, elution solvent 0.1 % FA in 50 % ACN) and the peptides dried in a vacuum concentrator prior to liquid chromatography-coupled mass spectrometry (LC-MS) analysis. For the membrane samples Fe^{3+}-IMAC was performed as described previously with some adjustments.[63] SepPac desalted peptide samples were re-suspended in ice-cold IMAC loading buffer (0.1 % TFA, 40 % acetonitrile). For quality control, 1.5 nmol of a synthetic library of phosphopeptides and their corresponding non-phosphorylated counterpart sequence (B2 and F1)[64] were spiked into each sample prior to loading onto a Fe^{3+}-IMAC column (Propac IMAC-10 4x50 mm, Thermo Fisher Scientific). The enrichment was performed with Buffer A (0.07 % TFA, 30 % acetonitrile) as wash buffer and Buffer B (0.315 % NH_4OH) as elution buffer. Collected full proteome and phosphopeptide fractions were vacuum-dried, reconstituted in 0.1 % FA or 0.1 % Fa, 50 mM citrate, respectively, desalted on self-packed stage tips and dried down prior to LC-MS analysis.

LC-MS/MS measurement

Dry peptides were re-suspended in 0.1 % FA in HPLC grade water and spiked with PROCAL retention time standard peptide.[65] LC-MS/MS analysis was performed on a Q Exactive HF Orbitrap (Thermo Fisher Scientific) coupled on-line to a Dionex Ultimate 3000 RSLCnano system. The liquid chromatography setup consisted of a 75 μm x 2 cm trap column and a 75 μm x 40 cm analytical column, packed in-house with Reprosil-Pur C18 ODS-3 5 μm or Reprosil Gold C18 3 μm resin (Dr. Maisch GmbH), respectively. Peptides were loaded onto the trap column using 0.1 % FA in water at a flow rate of 5 μL/min and separated using a 50 min linear gradient from

4 % to 32 % of solvent B (0.1 % (v/v) formic acid, 5 % (v/v) DMSO in acetonitrile) at 300 nL/min flow rate. nanoLC solvent A was 0.1 % (v/v) formic acid, 5 % (v/v) DMSO in HPLC grade water.[66] A 50 min two step gradient from 4 % to 27 % solvent B was used for the phosphoproteome samples.

Peptides were ionized using a spray voltage of 2.2 kV and a capillary temperature of 275 °C. The instrument was operated in data-dependent mode, automatically switching between MS1 and MS2 scans. Full scan MS1 spectra (m/z 360 – 1300) were acquired with a maximum injection time of 10 msec at 60,000 resolution and an automatic gain control (AGC) target value of 3e6 charges. For the top 20 precursor ions, high resolution MS2 spectra were generated in the Orbitrap with a maximum injection time of 25 msec at 15,000 resolution (isolation window 1.7 m/z), an AGC target value of 1e5 and normalized collision energy of 25 %. The underfill ratio was set to 1 % with a dynamic exclusion of 20 sec. Only precursors with charge states between 2 and 6 were selected for fragmentation. For the phosphoproteome analysis, the top 15 MS2 spectra were acquired with a maximum injection time of 100 msec, an AGC target value of 2e5 and a dynamic exclusion of 25 s.

(Phospho)proteomic data analysis

Thermo raw files for membrane full proteome and phosphoproteome samples were processed together as two separate parameter groups using MaxQuant software (v. 1.6.3.3) with standard settings unless otherwise described.[67] MS/MS spectra were searched against Araport11[68] protein coding genes (Araport11_genes.201606.pep.fasta; download 06/2016), the Xenopus reference proteome (UP00186698; uniprot download 05/2018) and spike-in phosphopeptide and PROCAL peptide library sequences,[64,65] with trypsin as protease and up to two allowed missed cleavages. Carbamidomethylation of cysteines was set as fixed modification and oxidation of methionine and N-terminal acetylation as variable modifications. For the phosphoproteome parameter group phosphorylation of serine, threonine or tyrosine was added as variable modification. Results were filtered to 1% PSM, protein and Site FDR. Raw data files for the cytoplasm proteome were processed in a separate MaxQuant search using the same settings as for the membrane full proteome.

For protein abundance comparisons PIN1 (AT1G73590), PIN2 (AT5G57090), PIN3 (AT1G70940), D6PK (AT5G55910) and PINOID (AT2G34650) LFQ peptide intensities were summed up for the respective samples and length corrected with the number of iBAQ peptides. Phosphorylation site intensities were normalized with the total peptide intensity (allPeptides.txt) ratio of the respective sample and filtered for sites identified with two valid values per grouping. Statistic comparison of D6PK and PINOID phosphorylation was performed in Perseus using Student T-test with standard settings (missing values imputed from normal distribution, 1.8 downshift, 0.3 width, separately for each column; s0=0; Permutation based FDR 0.05).[69]

Plant transformation and genotyping

Plants were transformed using *Agrobacterium tumefaciens* GV3101 according to.[70] In order to select for positive transformants, the seeds were sprayed with a Basta solution (1 % v/v). Seedlings that survived the treatment were transferred to single pots and genotyped by PCR. Primer sequences for genotyping are reported in Table S3.

Immunocytochemical techniques

Localization of proteins by immunocytochemical techniques was performed as described.[71,72] Antibodies were used as published previously.[73]

Modeling of IAA distribution in roots

Auxin dynamics were modeled on a two-dimensional cross section of an idealized *Arabidopsis thaliana* root tip anatomy containing at its distal end a quiescent center, surrounded by stem cell niche, columella, and root cap, and shootward from the QC consisting of epidermal, cortical, endodermal, pericycle and multiple vascular tissue cell files (from inside to outside). The model incorporates experimentally derived cell type and root zone specific patterns of the AUX/LAX auxin importers, the polarly localized PIN auxin exporters, and in addition to baseline cell level auxin production and degradation elevated levels of auxin production around the QC, in the columella and lateral root cap, as done previously.[5,26,74] Under standard model settings[5] PIN efflux rates are equal across all cell types and hence PIN types. Taking PIN2 transport rates as a default, we modeled the faster PIN3 mediated auxin transport by elevating columellar PIN efflux rates 8-fold, whereas to model the 2-fold higher transport rate of PIN1 we elevated vascular and pericycle PIN efflux rates 2-fold. Epidermal, cortical and endodermal PIN efflux rates were kept identical to standard settings.

In simulations of gravitropic stimulation, columellar PIN3 patterns were polarized to simulate their reorientation in response to statolith sedimentation.[75] In contrast to the default apolar PIN pattern in these cells, downward oriented membrane faces received 1.5 times more PINs whereas all other membrane faces received 0.3-fold lower PIN levels.

To simulate the *pin2* mutant, PIN levels in lateral root cap, epidermis and cortex were reduced to 0.1-fold their original value, reflecting that in *pin2* mutants there is a partial takeover by PIN1 becoming active in the PIN2 domain with correct polarity yet insufficiently to restore gravitropic response.[7] To simulate *PIN2* promotor mediated *PIN1* expression in *pin2* mutants, we replaced the polar PIN2 pattern with an apolar PIN1 pattern in epidermis and cortex. To simulate *PIN3* expression in the *PIN2* domain in *pin2* mutants, we replaced the polar PIN2 pattern with an apolar PIN3 pattern in epidermis and cortex and increased local PIN transport rates 8-fold.

The model is grid based, meaning individual cells and cell walls consist of a collection of grid points, and auxin dynamics are modeled as a partial differential equation. Grid based auxin dynamics were solved using an Alternating Direction Implicit (ADI) integration scheme, using a time step of 0.2 s and a space step of 2 microm, again as was done before[5,26,74]

Gravitropism and root growth assays

Sterilized seeds of Col-0, *pin2* mutant and the PIN T-DNA line were plated in two sets of 10 seeds per genotype on the plate containing 0.5 MS + 1 % sucrose. In order to minimize plate effects, the position of the genotypes was rotated on different plates, resulting in six plates and 120 seeds for each genotype per investigated PIN rescue line. The plates were sealed and incubated in the dark at 4 °C for two days. Afterwards the plates were placed vertically into a plant growth chamber and scanned 5 days later. The root angle between the root origin and the root tip was measured for every seedling, using the SNT plugin of FIJI and a script to give the value of the root angle simultaneously.[76,77] For each PIN construct, 5-10 individual segregating T2 lines were analyzed as described before. One representative line was propagated to the next generation, in order to generate a homozygous line. The representative homozygous PIN T-DNA line was plated with wildtype and mutant seedlings on the same plates with only one plate per plate layout (n = 60 seeds). The plates were processed as described earlier. The VGI of the homozygous lines was calculated using FIJI.[34] For root growth rate assays sterilized seeds were plated in two sets of 20 seeds per genotype on the plate containing 0.5 MS + 1 % sucrose. The plates were sealed and incubated in the dark at 4 °C for two days. Afterwards the plates were placed vertically into a plant growth chamber and growth rate monitored for 7 days. The root length was measured for every seedling, using the SNT plugin of FIJI and a script to give the value of the root length simultaneously.

Root bending assay

The homozygous PIN T-DNA lines of interest, the wildtype Col-0 and the *pin2* mutant were grown on plates containing the indicated medium for five days, after two days of stratification at 4 °C in the dark. Two times five seedlings were transferred to a new plate containing medium as indicated (either 0.5 MS + 1 % sucrose, or 0.5 MS without vitamins) and the root was straightened. The plate was turned 90 ° and was placed into a growth chamber (Sanyo, Moriguchi, Japan), together with an IR LED light module. A Raspberry Pi (Raspberry Pi Foundation, UK) equipped with an IR camera was placed in front of the plate and an image was taken every five minutes. The angle between the root body and the tip was measured every hour from 1-10 hours after turning and after 16 h.

GUS staining

The seeds of homozygous PIN T-DNA lines, the wildtype Col-0 and the *pin2* mutant were grown on plates containing 0.5 MS + 1 % sucrose for five days, after two days of stratification at 4 °C in the dark. The whole seedlings were transferred to a 6-well plate containing GUS staining solution (100 mM $NaPO_4$ pH 7.0, 100 mM EDTA pH 7.0, 1 mM $K_3[Fe(CN)_6]$, 1 mM $K_4[Fe(CN)_6]\cdot 3H_2O$, 0.1 % Triton X-100 in H_2O, 0.5 mg/ml X-Gluc in DMF) and incubated for 1 h at 37 °C with the plate covered in aluminum foil. Afterwards the seedlings were washed three times in buffer (50 mM $NaPO_4$ pH 7.0). The roots were mounted in chloral hydrate solution (50 % (w/v) chloral hydrate, 10 % (v/v) glycerol) and imaged at an Olympus BX61 Upright microscope (Hamburg, Germany).

Microscopy and signal quantification

In order to image the PIN localization in Arabidopsis roots or to image the R2D2 auxin reporter, an Olympus BX61 microscope with a FV1000 confocal laser scanning unit (Olympus, Hamburg, Germany) or a Leica TCS SP8 confocal microscope (Leica, Wetzlar, Germany) were used. The scale bar was automatically included using FIJI. All measurements for the polarity index or the R2D2 signal analysis were performed in FIJI.

The polarity index was determined by calculating the ratio of the GFP signal at the apical and lateral PM of root epidermal cells. A square (3 px x 15 px) was defined as region of interest (ROI) and four cells from two roots of three independent segregating lines were analyzed per genotype.

In order to analyze the R2D2 signal,[38] a maximum projection of 3–8 images with 2.0 μm intervals of either the epidermal or cortical cell file was used. A round ROI covered the nucleus. The R2 (mDII signal) to D2 (DII signal) ratio was calculated of the first five cells after the anticlinal division of the epidermis/lateral root cap initial cell (Q) and five cells at the transition zone (T). The GUS-stained roots were imaged at an Olympus BX61 Upright microscope (Hamburg, Germany).

QUANTIFICATION AND STATISTICAL ANALYSES

All data were plotted with GraphPad Prism V10.2.3 (Boston, USA). Statistical tests as indicated were performed using the default settings of GraphPad Prism V10.2.3. for detailed results of statistical tests see Table S2.